

Supporting Information for

Nitrogen-Doped Phosphorene for Electrocatalytic Ammonia

Synthesis

Guangrui Xu,^{a,b†} Hao Li,^{c†} Abdulaziz S. R. Bati,^d Munkhjargal Bat-Erdene,^d Md J. Nine,^e
Dusan Losic,^e Yu Chen,^{a*} Joseph G. Shapter,^{d*} Munkhbayar Batmunkh,^{d,f*} and Tianyi Ma,^{b*}

^a Key Laboratory of Macromolecular Science of Shaanxi Province, School of Materials Science and Engineering, Shaanxi Normal University, Xi'an 710062, China. E-mail: ndchenyu@gmail.com

^b School of Environmental and Life Sciences, The University of Newcastle (UON), Callaghan, New South Wales 2308, Australia. E-mail: tianyi.ma@newcastle.edu.au

^c Department of Chemistry, The University of Texas at Austin, Austin, TX, 78712, USA

^d Australian Institute for Bioengineering and Nanotechnology, The University of Queensland, Brisbane, Queensland 4072, Australia. E-mail: j.shapter@uq.edu.au

^e School of Chemical Engineering and Advanced Materials, The University of Adelaide, Adelaide, South Australia 5005, Australia.

^f Centre for Clean Environment and Energy, Griffith University, Gold Coast, Queensland 4222, Australia. E-mail: m.batmunkh@griffith.edu.au

† These two authors made an equal contribution to this work.

Experimental

Sample preparation (phosphorene, O-phosphorene and N-phosphorene)

Non-doped phosphorene dispersion (termed "phosphorene") was prepared in anhydrous N-Methyl-2-pyrrolidone (NMP) using a microwave (MW)-assisted liquid-phase exfoliation (LPE) method according to our previously established method.^{1, 2} This method includes two-step microwaving processes using two different types of MW instruments namely StartSYNTH Microwave Synthesis Labstation, Milestone s.r.l (with a maximum power of 600 W) and CEM Discover SP – MW (with a maximum power of 220 W). However the actual power applied is temperature dependent. The temperatures used for the StartSYNTH Microwave and CEM Discover SP were 50 °C for 8 min and 70 °C for 3 min, respectively. Then the solution was centrifuged at 6000 rpm for 30 min. Except the LPE in a microwave system and centrifugation, all experimental steps were carried out in a N₂-filled glove box to control the BP oxidation.

Oxygen-doped and nitrogen-doped phosphorene dispersions (termed "O-phosphorene" and "N-phosphorene") were prepared in anhydrous NMP solvent using a combination of ball milling and MW-assisted LPE method. Firstly, bulk BP crystals were ground using a mortar and pestle, followed by oxidization in air for 2 h. The oxidized bulk BP samples (50 mg) were put in a zirconia milling pot, to which 2 mL N-Methyl-2-pyrrolidone (NMP) solvent was added. The samples were then ball milled using Retsch planetary ball mills (PM 200) with zirconia balls (1 mm) at 300 rpm for 30 min. No doping agent was used during the ball milling for the O-phosphorene sample, while ammonium hydroxide aqueous solution (NH₄OH) as the N source was added in the milling pot for the N-phosphorene. The ratio of BP and doping agent was 1:5 (w/w %). After washing with isopropyl alcohol (IPA), the ball milled O-phosphorene and N-phosphorene were re-dispersed in NMP for further exfoliation. The exfoliations were carried using only StartSYNTH Microwave at 50 °C for 8 min. The supernatants were taken and centrifuged at 6000 rpm for 30 min.

Materials characterization

Atomic force microscopy (AFM) was performed in air using Asylum Research Cypher S with Asylum Research software, operating in standard tapping mode configuration using AIR cantilever holder. The AFM probe used was high accuracy noncontact composite probe with silicon body, polysilicon lever and silicon high resolution tip (tip curvature radius: <10 nm) from TipsNano. Set-point, drive-amplitude, scan rate and gain values were tuned to

optimize image quality and flake thickness. The AFM topography images have been flattened and thickness measurements were made using the section analysis tool of Asylum Research software.

Raman spectra were acquired using a WITec alpha300 RA+S Raman microscope using an excitation laser wavelength of 532 nm with a 20x objective. The grating used was 600 grooves mm^{-1} . The excitation laser power levels were kept as low as possible to prevent sample damage. For Raman analysis, the samples were prepared by drop casting the solution onto silicon substrates. UV-vis absorption of the phosphorene dispersions was studied using a UV-vis spectroscopy (Shimadzu UV-2600) at wavelength ranging from 200 nm to 800 nm with an interval of 1 nm.

XPS data were acquired using a Kratos Axis ULTRA X-ray Photoelectron Spectrometer incorporating a 165 mm hemispherical electron energy analyzer. The incident radiation was monochromatic Al K_{α} X-rays (1486.6 eV) at 225 W (15 kV, 15 mA). Survey scans were collected at an analyzer pass energy of 160 eV while high-resolution (HR) scans were at 20 eV. Survey scans were carried out at binding energies between 1200 eV and 0 eV with 1.0 eV steps and 100 ms dwell time. HR scans were run with 0.05 eV steps and 250 ms dwell time. Base pressure in the analysis chamber was 1.0×10^{-9} Torr and during sample analysis 1.0×10^{-8} Torr. The samples for the XPS analysis were prepared by drop casting the solution onto silicon substrates.

Bright-field transmission electron microscopy (TEM) images were acquired using a FEI Titan Themis. Samples were dispersed by drop-casting onto quantifoil SQR12-200CU grids, and transferred to high vacuum storage prior to analysis. Scanning transmission electron microscopy (STEM) imaging and Energy-Dispersive X-ray (EDX) elemental mapping were carried out also on a FEI Titan Themis S-TEM instrument. The STEM probe was aberration corrected, enabling sub-angstrom spatial resolution, and High Angle Annular Dark Field (HAADF) images were obtained.

Electrochemical measurements

All electrochemical measurements were performed on CHI 760E electrochemical workstation with a gas-tight H-type cell (80 mL in each cell compartment) separated by a piece of Nafion 117 membrane. Before a nitrogen reduction test, the Nafion membrane was protonated by boiling in DI water, in H_2O_2 , in DI water for 1 h, respectively, and then boiling in 0.5 M H_2SO_4 for 3 h, and finally boiling in DI water for 6 h. Ag/AgCl electrode and carbon rod were used as

the counter electrode and reference electrode, respectively. The working electrode was prepared by dispersing catalysts on a copper foam (CF) with an area of $1 \times 1 \text{ cm}^2$. The mass loading of BP catalyst on CF was about 0.3 mg. The linear sweep voltammetry (LSV) was performed in 0.1 M KOH solution at a scan rate of 10 mV s^{-1} . NH_3 was generated by chronoamperometry at different potentials with N_2 gas continuously injected into the cathodic compartment by using a properly positioned sparger. The electrolyte was purged with N_2 for 0.5 h before measurement. All electrochemical analyses were performed without iR correction. Detailed descriptions of product analysis including determination of the produced NH_3 and N_2H_4 can be found in the supporting information.

Product analysis

Determination of the produced ammonia

The generated NH_3 was quantitatively determined using an ammonia selective electrode (Thermo Scientific) and the indophenol blue method.^{3, 4} These two methods can be used to measure the ammonia in the examination of water and wastewater in which the ammonia concentration may be lower than 10 ppm.

Procedures of ammonia selective electrode method:

- i) A series of standard solutions were prepared with the concentrations 0.02 ppm, 0.2 ppm, 2 ppm of NH_4Cl in 0.1 M KOH solution.
- ii) The meter measurement mode changed to mV mode, and the electrode soaked in 50 mL 0.1 M KOH solution with 1 mL alkaline reagent for 15 min for adapting to the environment.
- iii) 50 mL of each standard solution with 1 mL alkaline reagent was measured under the same conditions. The measurement was then recorded after stabilizing the solutions.
- iv) The mV value and $\lg(\text{ppm})$ were used as Y- and X-axis, respectively, to prepare the standard curve (the slope should be between 54 and 60 in a temperature range of 20-25 °C) (Fig. S8).
- v) 50 mL of the electrolyte with 1 mL alkaline reagent was measured under the same conditions. The measurement was then recorded after stabilizing the solutions.
- vi) Calculating the NH_3 yields and FEs.

Procedures of the indophenol blue method:

- i) Preparation of reagents used:
 - a. Phenol-alcohol reagent: dissolve add 10 g of phenol in 95% ethyl alcohol to a final volume of 100 mL.
 - b. Sodium nitroprusside (nitroferricyanide): dissolve 1 g in DI water to a final volume of 200 mL.
 - c. Alkaline complexing reagent: dissolve 100 g of trisodium citrate and 5 g of sodium hydroxide in DI water to a final volume of 500 mL.
 - d. Sodium hypochlorite: use commercial bleach (i.e., Chlorox).
 - e. Oxidizing solution: add 100 mL alkaline solution to 25 mL sodium hypochlorite. Prepare fresh daily.
- ii) Preparation of a series of standard ammonium solutions.
- iii) 10 mL of aliquot of the solution was taken out. Then 400 μ L of phenol-alcohol reagent, 400 μ L of sodium nitroferricyanide and 500 μ L of oxidizing solution were added to the sample solution. Absorbance measurements were performed at 650 nm after 3 h.
- iv) The absorbance value and concentration (ppm) of the ammonia were plotted in the Y- and X-axis, respectively, to prepare the standard curve (Fig. S9).
- v) 10 mL of the electrolyte solution was removed from the electrochemical reaction vessel. Then 400 μ L of phenol-alcohol reagent, 400 μ L of sodium nitroferricyanide and 500 μ L of oxidizing solution were added to the above solution. Absorbance measurements were performed at 650 nm after 3 hours of stabilization.
- vii) Calculating the NH_3 yields and FEs.

The equation of the equilibrium potential:

$$E = E^\theta - RT/6F \times \ln([\text{NH}_4\text{OH}]^2/[\text{H}^+]^6) + 0.059 V \times pH \quad (1)$$

The equation of mass-normalized yield rate of NH_3 :

$$\text{NH}_3 \text{ yield rate} = (c_{\text{NH}_3} \times V) / (m \times t) \quad (2)$$

The equation of FE of NH_3 production:

$$FE = 3F \times c_{\text{NH}_3} \times V / (17 \times Q) \times 100\% \quad (3)$$

where E^θ is 0.092 V, the universal gas constant R is 8.314 J K⁻¹ mol⁻¹, T is the temperature in Kelvin, F is the Faraday constant (96485 C mol⁻¹), c_{NH_3} is the sum of the NH_3 concentration in 0.1 M KOH solution, V is the volume of electrolyte, t is the reduction reaction time, A is the surface area of the working electrode, and Q is the total charge passed through the electrodes during the reaction duration according to total current density.

Determination of the produced hydrazine

i) Preparation of reagents used:

Color reagent: Preparing color reagent by mixing p-dimethylaminobenzaldehyde (5.99 g), ethanol (300 mL) and HCl (concentrated, 30 mL).

ii) Preparation of a series of standard hydrazine solutions.

iii) 10 mL of aliquot of the solution was taken out, to which 5 mL color reagent was added. Absorbance measurements were performed at 450 nm.

iv) The absorbance value and concentration (ppm) of hydrazine were plotted as Y-axis and X-axis respectively, to prepare the standard curve (Fig. S10).

v) 10 mL of the electrolyte solution was taken out to which 5 mL color reagent was added. Absorbance was performed at 450 nm after stirring for 15 min at room temperature.

vi) Calculation the N_2H_4 yield.

Computational and modeling methodology

Density functional theory (DFT) calculations were performed using the VASP code. The electronic exchange and correlation were described by the generalized gradient approximation (PAW) method;⁵ the Perdew–Burke–Ernzerhof (PBE) functional was employed. The valence electrons were described by the Kohn–Sham (KS) wave functions being expanded in a plane wave basis with the energy cutoff of 400 eV.⁶ The core electrons were described by the projector augmented-wave (PAW) method.⁷ Van der Waals corrections were applied using a DFT-D3 method.⁸ Geometries were considered fully relaxed after all the forces fell below 0.05 eV per Å. A $(3 \times 3 \times 1)$ Monkhorst–Pack (MP) k -point mesh was employed to sample the Brillouin zone.⁹ Layered phosphorene structures with 4-layers were modelled for the study. The N and O doped surfaces were modelled by replacing a P in the layer with N or O.

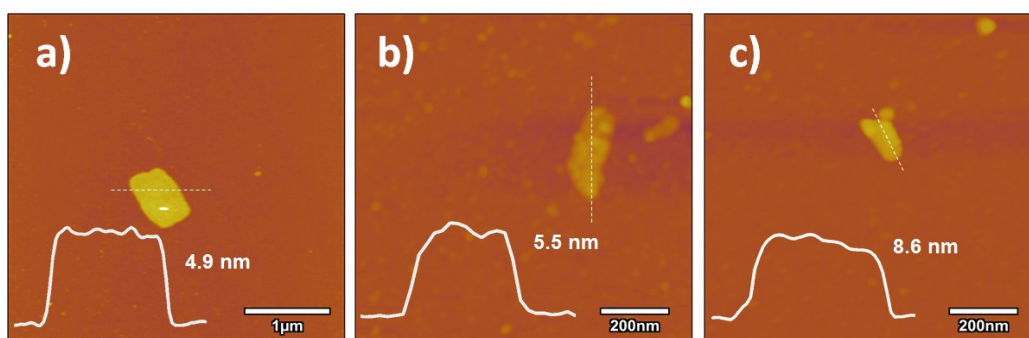


Fig. S1 AFM images of (a) non-doped, (b) O-doped and (c) N-doped phosphorene

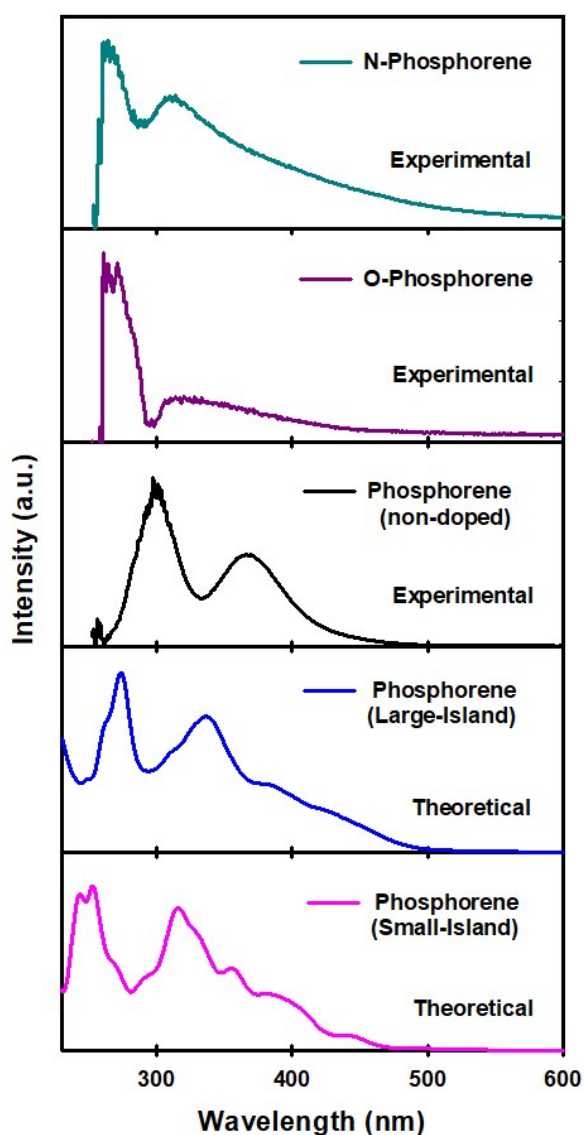


Fig. S2 Experimentally measured UV-vis spectra of non-doped, O-doped and N-doped phosphorene dispersions; and theoretically simulated UV-vis spectra of phosphorene with small and large flake sizes. Density-functional theory (DFT) calculation data are reproduced from ref.¹.

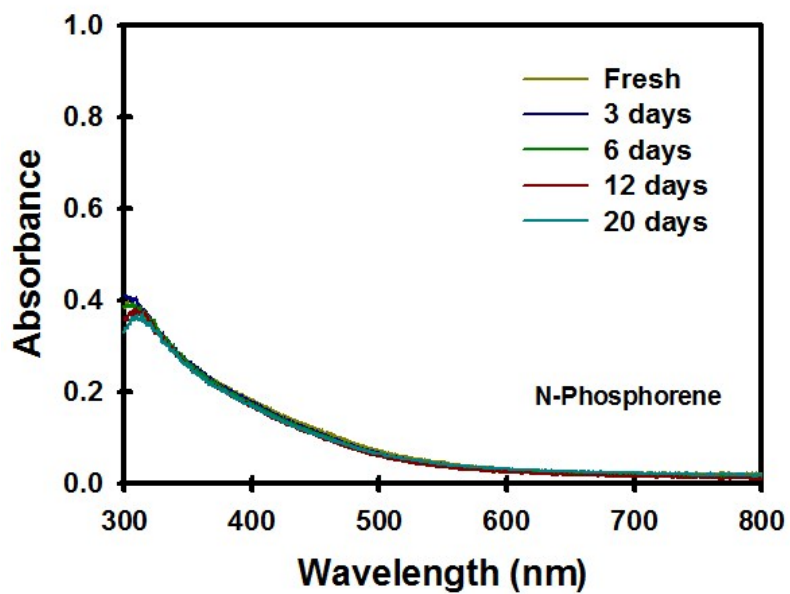


Fig. S3 UV-vis spectra of N-phosphorene dispersion over 20 days.

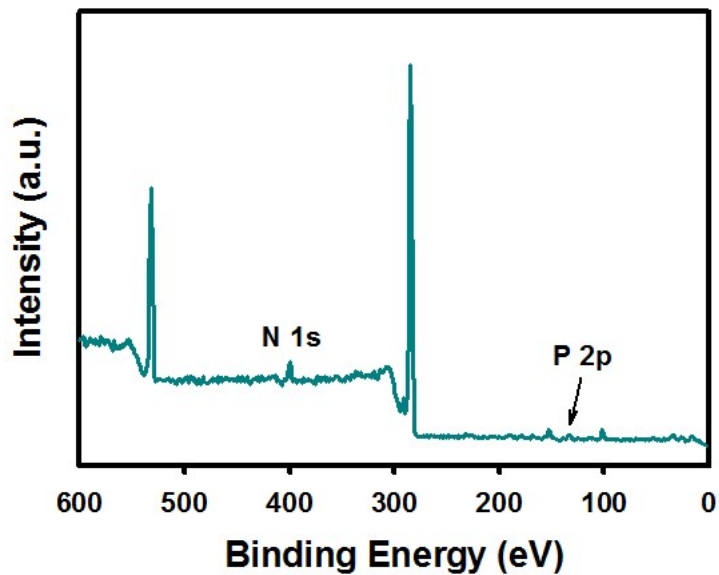


Fig. S4 XPS survey spectrum of N-phosphorene nanosheets.

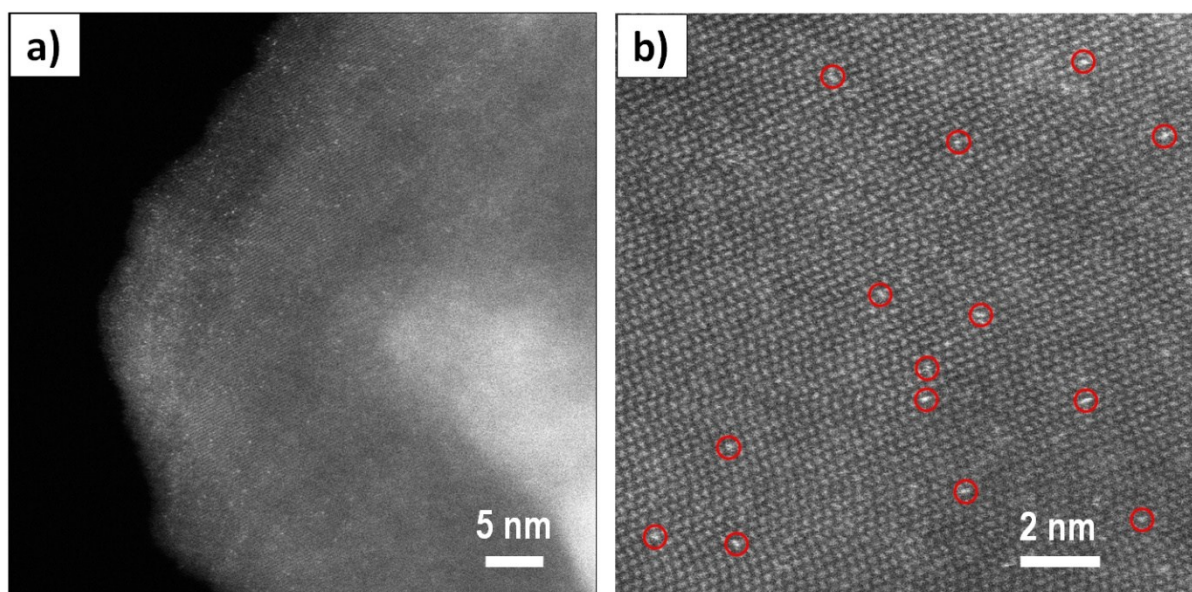


Fig. S5 HRTEM images of N-phosphorene nanosheet. Ultrasmall atomic size dots (circled by red) can be observed due to the significant functionalization and doping.

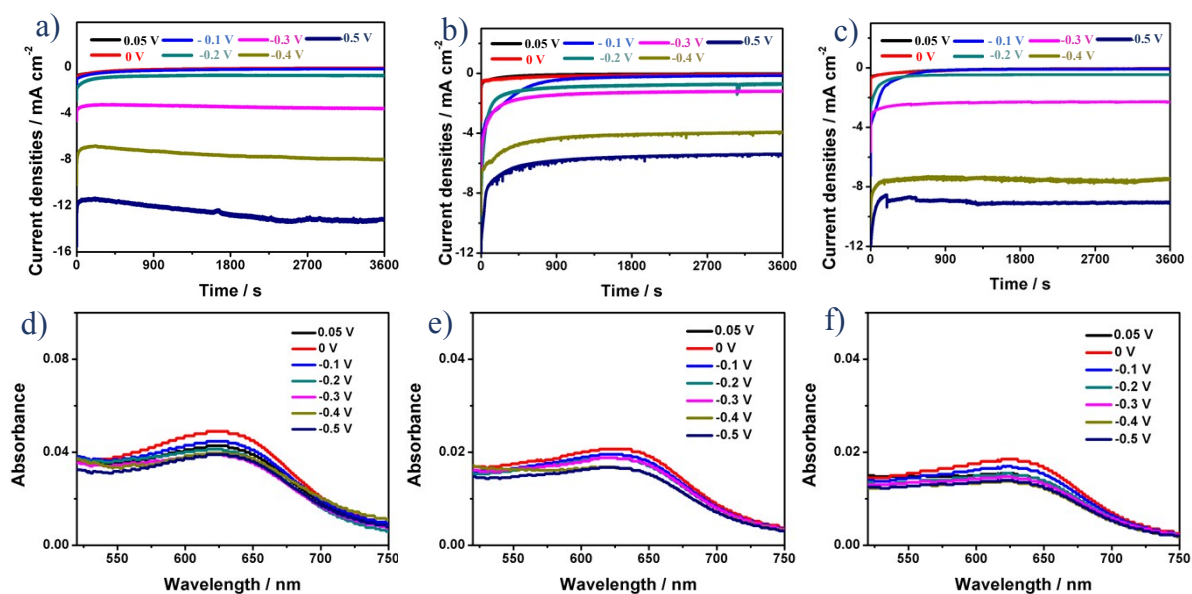


Fig. S6 Chronoamperometric curves of (a) N-phosphorene, (b) O-phosphorene and (c) phosphorene in N_2 -saturated 0.1 M KOH electrolyte at different potentials. UV-visible absorption spectra of the electrolytes treated with indophenol blue after electrolysis in the presence of (d) N-phosphorene, (e) O-phosphorene and (f) phosphorene at different potentials for 1 h.

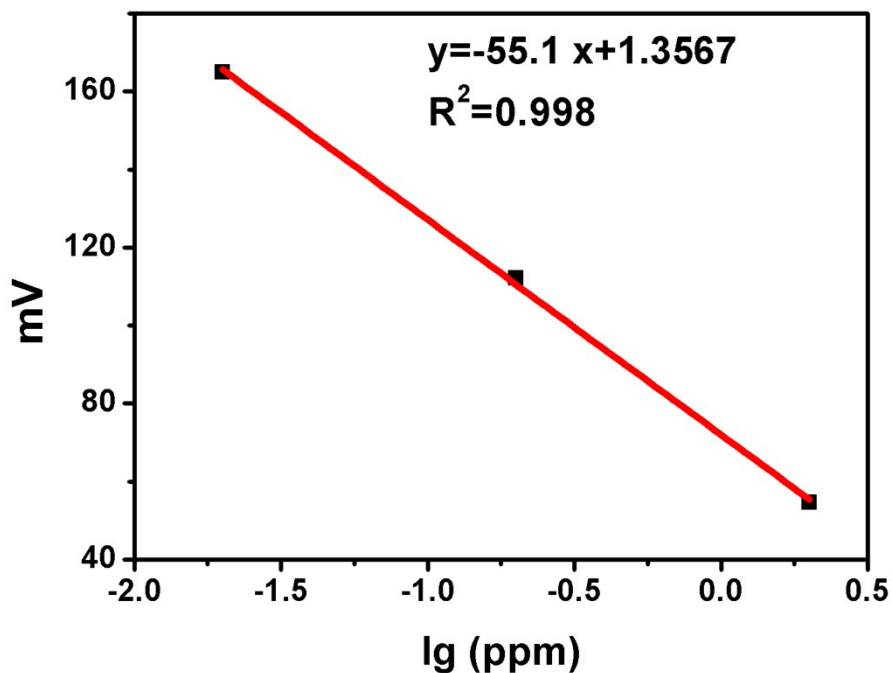


Fig. S7 Calibration of NH_3 in 0.1M KOH from 0.02 ppm to 2 ppm. The fitting curve shows good linear relation of mV with $\log(\text{NH}_4^+$ ion concentration) ($y = -55.1x - 3.0311$, $R^2 = 0.998$).

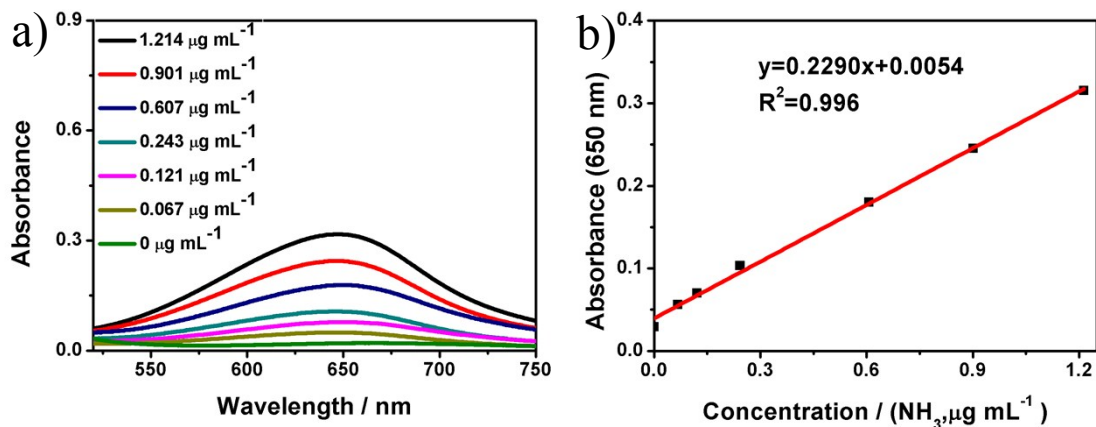


Fig. S8 Determination of the produced NH_3 in 0.1 M KOH. (a) UV-vis absorption spectra of the electrolytes treated with indophenol blue for 3 hr and (b) the corresponding calibration curve for the colorimetric NH_3 assay using the indophenol blue method in 0.1 M KOH. The absorbance at 650 nm was used for the calibration, and the fitting curve shows good linear relation of absorbance with NH_4^+ ion concentration ($y = 0.2154x - 6 \times 10^{-4}$, $R^2 = 0.999$) of three times independent calibration curves.

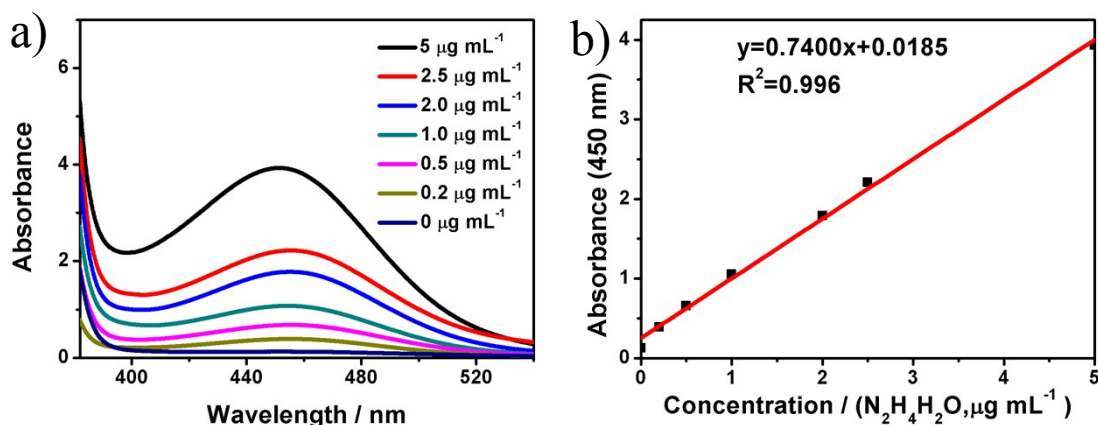


Fig. S9 Determination of the produced $\text{N}_2\text{H}_4 \cdot \text{H}_2\text{O}$ in 0.1 M KOH. (a) UV-vis absorption spectra of standard hydrazine solutions after mixing p-dimethylaminobenzaldehyde and (b) the corresponding calibration curve for the colorimetric N_2H_4 assay using the Watt and Chrisp method. The absorbance at 450 nm was used for the calibration, and the fitting curve shows good linear relation of absorbance with $\text{N}_2\text{H}_4 \cdot \text{H}_2\text{O}$ concentration ($y=0.7400x+0.0185$, $R^2=0.996$) of three times independent calibration curves.

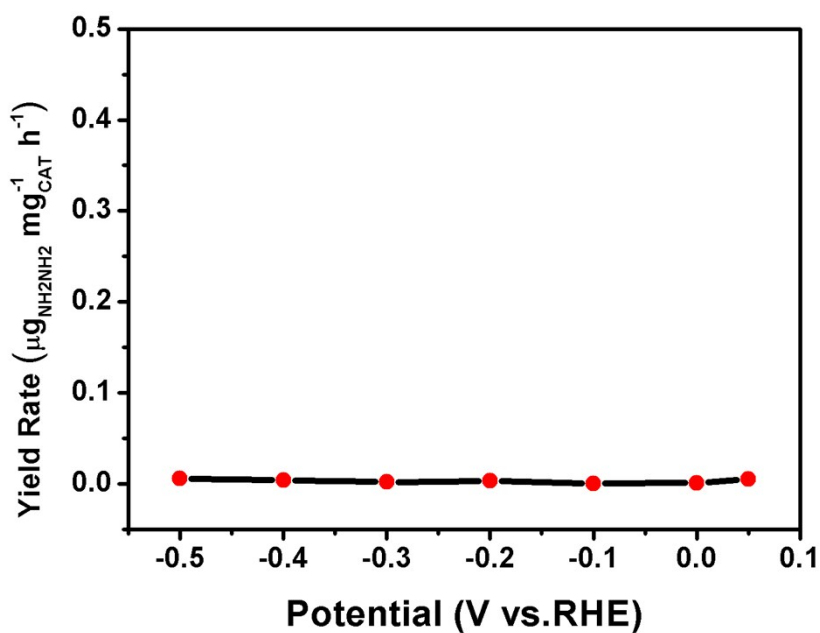


Fig. S10 The yield rate of $\text{N}_2\text{H}_4 \cdot \text{H}_2\text{O}$ at different potentials.

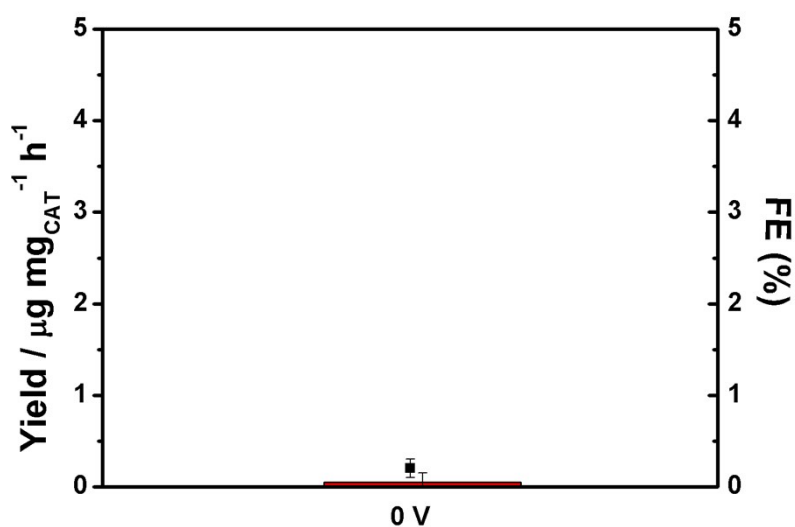


Fig. S11 NH_3 yield rate and Faradaic efficiency (FE) of N-phosphorene nanosheets in Ar-saturated at 0 V vs. RHE for 1 h. When the reaction proceeded in Ar-saturated electrolyte at 0 V for 1 h, the NH_3 yield rate and FE using N-phosphorene nanosheets were negligible compared to that of N-phosphorene in N_2 -saturated electrolyte.

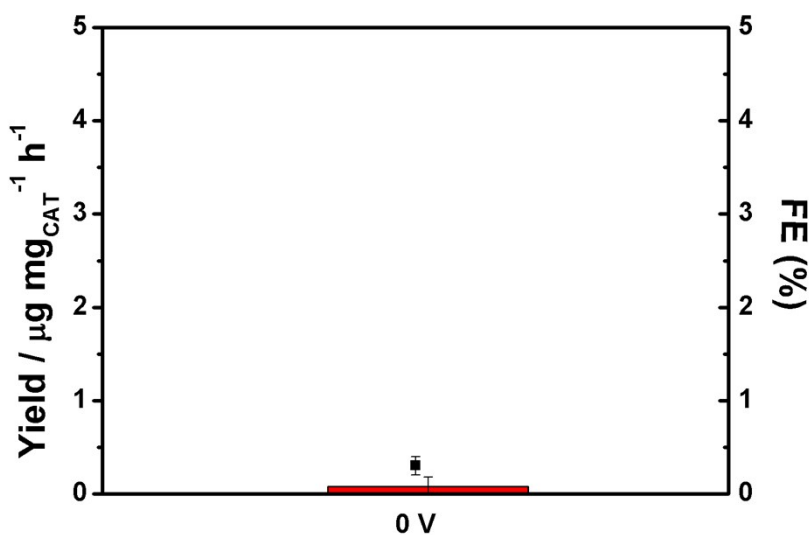


Fig. S12 NH_3 yield rate and FE of a pure CF in N_2 -saturated at 0 V for 1 h. After the reaction proceeded in N_2 -saturated electrolyte with a pure CF at 0 V vs. RHE for 1 h, the NH_3 yield rate and FE were negligible in comparison to that of N-phosphorene under N_2 -saturated.

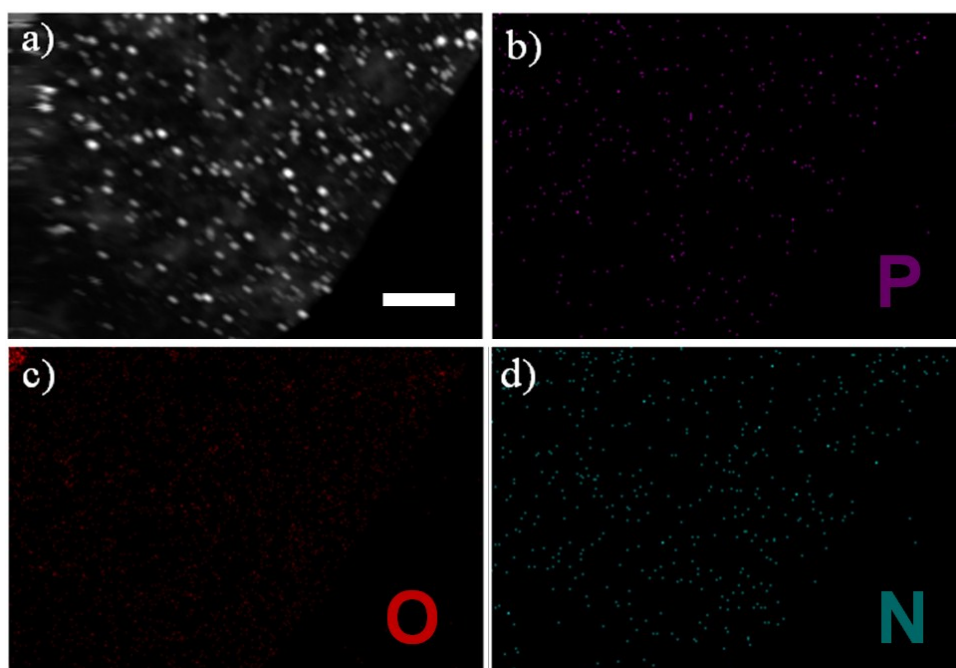


Fig. S13 (a) High-angle annular dark-field – scanning transmission electron microscope (HAADF–STEM) image of N-phosphorene nanosheet (scale bar: 1 μm), and (b-d) the corresponding EDX elemental mapping after six cycles of continuous NRR catalysis.

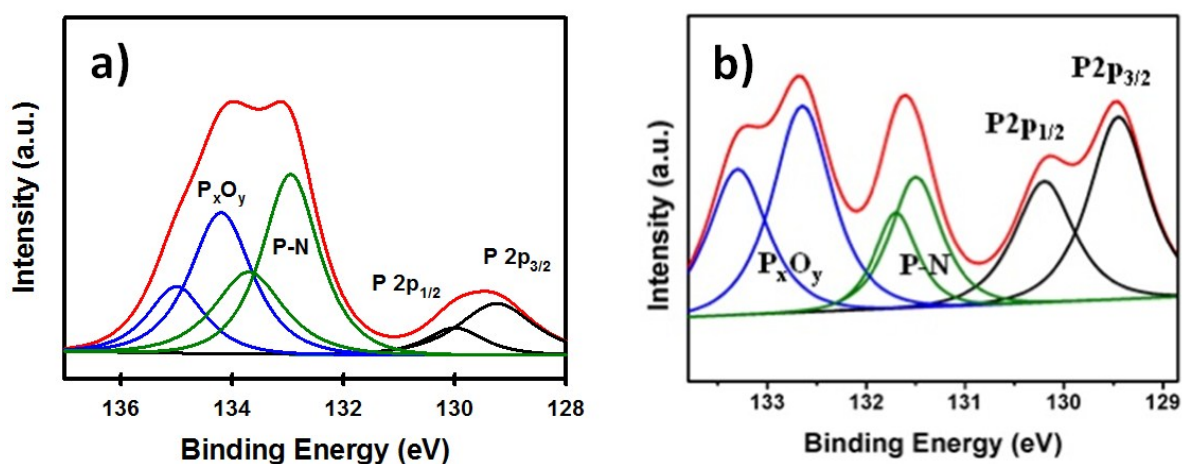


Fig. S14 High resolution P 2p XPS spectrum of N-phosphorene nanosheet (a) before catalysis and (b) after six cycles of continuous NRR electrocatalysis.

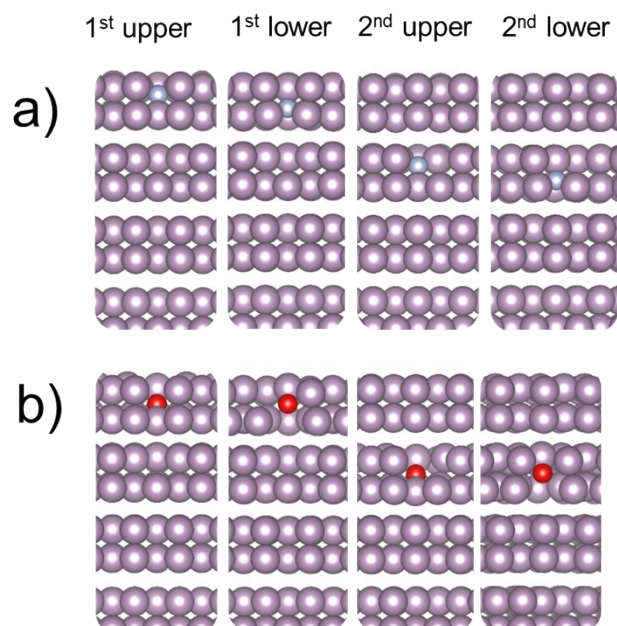


Fig. S15 DFT-optimized phosphorene geometries with different positions of the dopants (a) N and (b) O. Purple, blue, and red spheres represent P, N, and O, respectively.

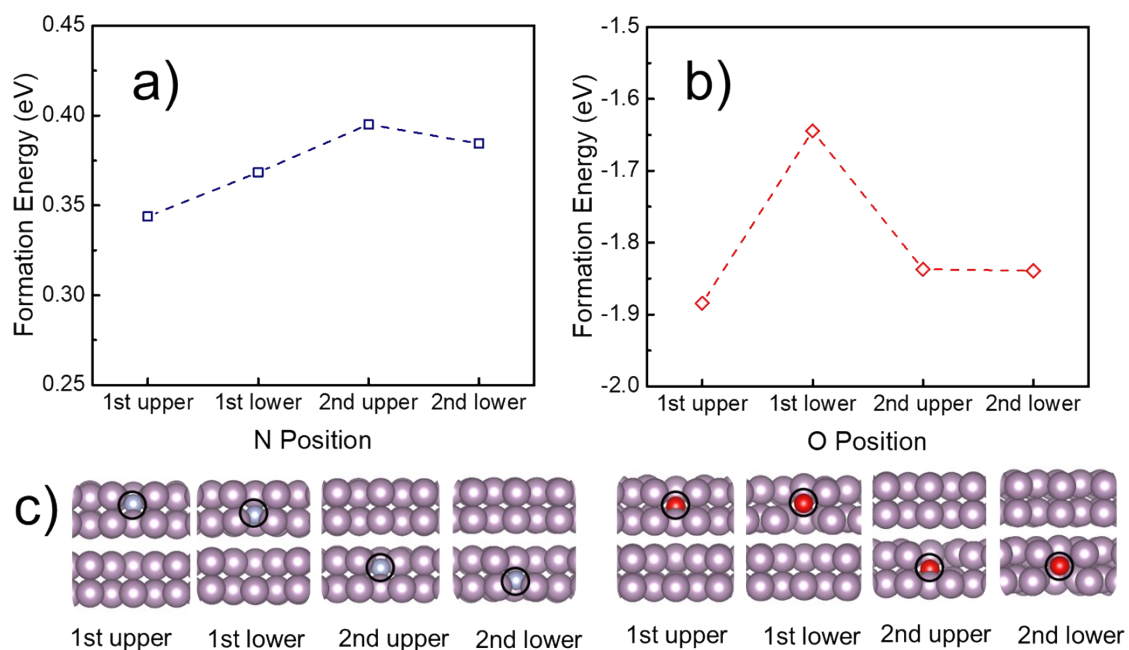


Fig. S16 Calculated formation energy of the phosphorene structure doped with (a) N and (b) O at different positions, with the optimized structures of the first two layers shown in (c). Purple, blue, and red spheres represent P, N, and O, respectively. The total energies of N_2 , O_2 , and P bulk structure were used as the energy references.

Table S1. Summary of NRR performances (NH₃ yield and FE) of different catalysts.

Catalyst	NH ₃ yield	FE (%)	Electrolyte	Overpotential (vs. RHE)	Ref
N-doped phosphorene (N-phosphorene)	18.79 $\mu\text{g h}^{-1}$ $\text{mg}^{-1}_{\text{CAT}}$	21.51	0.1 M KOH	0 V	This work
Tetrahexahedral gold nanorods (AuNRs)	1.648 $\mu\text{g h}^{-1}$ cm^{-2}	4.02	0.1 M KOH	-0.20 V	10
Au/TiO₂	21.40 $\mu\text{g h}^{-1}$ $\text{mg}^{-1}_{\text{CAT}}$	8.11	0.1 M HCl	-0.20 V	11
a-Au/CeO_x-RGO	8.30 $\mu\text{g h}^{-1}$ $\text{mg}^{-1}_{\text{CAT}}$	10.10	0.1 M HCl	-0.20 V	12
Au flowers	25.57 $\mu\text{g h}^{-1}$ $\text{mg}^{-1}_{\text{CAT}}$	6.05	0.1 M HCl	-0.20 V	13
Hollow gold nanocages (AuHNC)	3.90 $\mu\text{g h}^{-1}$ cm^{-2}	30.20	0.5 M LiClO ₄	-0.40 V	14
Pd/C	4.50 $\mu\text{g h}^{-1}$ $\text{mg}^{-1}_{\text{CAT}}$	8.20	0.1 M PBS	0.10 V	3
Ru@NC	3.665 $\mu\text{g h}^{-1}$ $\text{mg}^{-1}_{\text{CAT}}$	7.50	0.1 M HCl	-0.21 V	15
Ru nanoparticles	0.55 $\mu\text{g h}^{-1}$ cm^{-2}	5.40	0.01 M HCl	0.01 V	16
Ru/MoS₂	6.98 $\mu\text{g h}^{-1}$ $\text{mg}^{-1}_{\text{CAT}}$	17.60	0.01 M HCl	-0.15 V	17
Mo₂C	11.3 $\mu\text{g h}^{-1}$ $\text{mg}^{-1}_{\text{CAT}}$	1.10	0.5 M Li ₂ SO ₄	-0.30 V	18
Mo₂N nanorod	78.4 $\mu\text{g h}^{-1}$ $\text{mg}^{-1}_{\text{CAT}}$	4.50	0.1 M HCl	-0.30 V	19
MoO₂	12.20 $\mu\text{g h}^{-1}$ $\text{mg}^{-1}_{\text{CAT}}$	8.20	0.1 M HCl	-0.15 V	20
Fe/Fe₃O₄	0.19 $\mu\text{g h}^{-1}$ cm^{-2}	8.29	0.1 M PBS	-0.30 V	21
Defect-rich MoS₂ nanoflower	29.28 $\mu\text{g h}^{-1}$ $\text{mg}^{-1}_{\text{CAT}}$	8.34	0.1 M Na ₂ SO ₄	-0.40 V	22
Bismuth nanosheets (BiNSs)	13.23 $\mu\text{g h}^{-1}$ $\text{mg}^{-1}_{\text{CAT}}$	10.46	0.1 M Na ₂ SO ₄	-0.80 V	23
Bi₄V₂O₁₁/CeO₂	23.21 $\mu\text{g h}^{-1}$ $\text{mg}^{-1}_{\text{CAT}}$	10.16	HCl; pH=1	-0.20 V	24
Nb₂O₅ nanofiber	43.60 $\mu\text{g h}^{-1}$ $\text{mg}^{-1}_{\text{CAT}}$	9.26	0.1 M HCl	-0.55 V	25
CoP hollow nanocage	2.49 $\mu\text{g h}^{-1}$ $\text{mg}^{-1}_{\text{CAT}}$	7.36	1 M KOH	0 V	26
Fe-N-C	7.48 $\mu\text{g h}^{-1}$	56.55	1 M KOH	0 V	27

	$\text{mg}^{-1}_{\text{CAT}}$				
Bismuth nanocrystals (BiNCs)	$3400 \mu\text{g h}^{-1} \text{mg}^{-1}_{\text{CAT}}$	66	$0.5 \text{ K}_2\text{SO}_4$	-0.60 V	28
BiVO_4	$8.60 \mu\text{g h}^{-1} \text{mg}^{-1}_{\text{CAT}}$	10.04	$0.2 \text{ M Na}_2\text{SO}_4$	-0.50 V	29
Vanadium nitride (VN) nanoparticles	$3.30 \times 10^{-10} \text{ mol s}^{-1} \text{ cm}^{-2}$	6.0	$0.05 \text{ M H}_2\text{SO}_4$	-0.10 V	30
2D Layered W_2N_3	$11.66 \mu\text{g h}^{-1} \text{mg}^{-1}_{\text{CAT}}$	11.67	0.1 M KOH	-0.20 V	31
MXene	$4.72 \mu\text{g h}^{-1} \text{cm}^{-2}$	4.62	$0.5 \text{ M Li}_2\text{SO}_4$	-0.10 V	32
PEBCD	$1.58 \mu\text{g h}^{-1} \text{cm}^{-2}$	2.85	$0.5 \text{ M Li}_2\text{SO}_4$	-0.50 V	33
Black phosphorus (BP) nanosheets	$20.87 \mu\text{g h}^{-1} \text{mg}^{-1}_{\text{CAT}}$	5.07	0.01 M HCl	-0.60 V	34
Boron-doped graphene	$9.80 \mu\text{g h}^{-1} \text{cm}^{-2}$	10.80	$0.05 \text{ M H}_2\text{SO}_4$	-0.50 V	35
Polymeric carbon nitride	$8.09 \mu\text{g h}^{-1} \text{mg}^{-1}_{\text{CAT}}$	11.59	0.1 M HCl	-0.20 V	36
Boron carbide (B_4C)	$26.57 \mu\text{g h}^{-1} \text{mg}^{-1}_{\text{CAT}}$	15.95	0.1 M HCl	-0.75 V	37
B_4C/Boron-doped graphene QDs	$28.60 \mu\text{g h}^{-1} \text{mg}^{-1}_{\text{CAT}}$	16.70	0.1 M HCl	-0.45 V	38

References

1. M. Bat-Erdene, M. Batmunkh, C. J. Shearer, S. A. Tawfik, M. J. Ford, L. Yu, A. J. Sibley, A. D. Slattery, J. S. Quinton, C. T. Gibson and J. G. Shapter, *Small Methods*, 2017, **1**, 1700260.
2. M. Bat-Erdene, M. Batmunkh, S. A. Tawfik, M. Fronzi, M. J. Ford, C. J. Shearer, L. Yu, M. Dadkhah, J. R. Gascooke, C. T. Gibson and J. G. Shapter, *Adv. Funct Mater.*, 2017, **27**, 1704488.
3. J. Wang, L. Yu, L. Hu, G. Chen, H. Xin and X. Feng, *Nat Commun.*, 2018, **9**, 1795.
4. S. Chen, S. Perathoner, C. Ampelli, C. Mebrahtu, D. Su and G. Centi, *Angew. Chem. Int. Ed.*, 2017, **56**, 2699-2703.
5. J. P. Perdew, K. Burke and M. Ernzerhof, *Phys. Rev. Lett.*, 1996, **77**, 3865-3868.
6. W. Kohn and L. J. Sham, *Phys. Rev.*, 1965, **140**, A1133-A1138.
7. P. E. Blöchl, *Phys. Rev. B.*, 1994, **50**, 17953-17979.
8. J. Moellmann and S. Grimme, *J. Phys. Chem. C.*, 2014, **118**, 7615-7621.
9. H. J. Monkhorst and J. D. Pack, *Phys. Rev. B.*, 1976, **13**, 5188-5192.
10. D. Bao, Q. Zhang, F.-L. Meng, H.-X. Zhong, M.-M. Shi, Y. Zhang, J.-M. Yan, Q. Jiang and X.-B. Zhang, *Adv. Mater.*, 2017, **29**, 1604799.
11. M.-M. Shi, D. Bao, B.-R. Wulan, Y.-H. Li, Y.-F. Zhang, J.-M. Yan and Q. Jiang, *Adv. Mater.*, 2017, **29**, 1606550.
12. S.-J. Li, D. Bao, M.-M. Shi, B.-R. Wulan, J.-M. Yan and Q. Jiang, *Adv. Mater.*, 2017, **29**, 1700001.

13. Z. Wang, Y. Li, H. Yu, Y. Xu, H. Xue, X. Li, H. Wang and L. Wang, *ChemSusChem*, 2018, **11**, 3480-3485.
14. M. Nazemi, S. R. Panikkanvalappil and M. A. El-Sayed, *Nano Energy*, 2018, **49**, 316-323.
15. H. Tao, C. Choi, L.-X. Ding, Z. Jiang, Z. Han, M. Jia, Q. Fan, Y. Gao, H. Wang, A. W. Robertson, S. Hong, Y. Jung, S. Liu and Z. Sun, *Chem*, 2019, **5**, 204-214.
16. D. Wang, L. M. Azofra, M. Harb, L. Cavallo, X. Zhang, B. H. R. Suryanto and D. R. MacFarlane, *ChemSusChem*, 2018, **11**, 3416-3422.
17. B. H. R. Suryanto, D. Wang, L. M. Azofra, M. Harb, L. Cavallo, R. Jalili, D. R. G. Mitchell, M. Chatti and D. R. MacFarlane, *ACS Energy Lett.*, 2019, **4**, 430-435.
18. H. Cheng, L.-X. Ding, G.-F. Chen, L. Zhang, J. Xue and H. Wang, *Adv. Mater.*, 2018, **30**, 1803694.
19. X. Ren, G. Cui, L. Chen, F. Xie, Q. Wei, Z. Tian and X. Sun, *Chem. Commun.*, 2018, **54**, 8474-8477.
20. G. Zhang, Q. Ji, K. Zhang, Y. Chen, Z. Li, H. Liu, J. Li and J. Qu, *Nano Energy*, 2019, **59**, 10-16.
21. L. Hu, A. Khaniya, J. Wang, G. Chen, W. E. Kaden and X. Feng, *ACS Catal.*, 2018, **8**, 9312-9319.
22. X. Li, T. Li, Y. Ma, Q. Wei, W. Qiu, H. Guo, X. Shi, P. Zhang, A. M. Asiri, L. Chen, B. Tang and X. Sun, *Adv. Energy Mater.*, 2018, **8**, 1801357.
23. L. Li, C. Tang, B. Xia, H. Jin, Y. Zheng and S.-Z. Qiao, *ACS Catal.*, 2019, **9**, 2902-2908.
24. C. Lv, C. Yan, G. Chen, Y. Ding, J. Sun, Y. Zhou and G. Yu, *Angew. Chem. Int. Ed.*, 2018, **57**, 6073-6076.
25. J. Han, Z. Liu, Y. Ma, G. Cui, F. Xie, F. Wang, Y. Wu, S. Gao, Y. Xu and X. Sun, *Nano Energy*, 2018, **52**, 264-270.
26. W. Guo, Z. Liang, J. Zhao, B. Zhu, K. Cai, R. Zou and Q. Xu, *Small Methods*, 2018, **2**, 1800204.
27. M. Wang, S. Liu, T. Qian, J. Liu, J. Zhou, H. Ji, J. Xiong, J. Zhong and C. Yan, *Nat Commun.*, 2019, **10**, 341.
28. Y.-C. Hao, Y. Guo, L.-W. Chen, M. Shu, X.-Y. Wang, T.-A. Bu, W.-Y. Gao, N. Zhang, X. Su, X. Feng, J.-W. Zhou, B. Wang, C.-W. Hu, A.-X. Yin, R. Si, Y.-W. Zhang and C.-H. Yan, *Nat Catal.*, 2019, **2**, 448-456.
29. J.-X. Yao, D. Bao, Q. Zhang, M.-M. Shi, Y. Wang, R. Gao, J.-M. Yan and Q. Jiang, *Small Methods*, 2019, **3**, 1800333.
30. X. Yang, J. Nash, J. Anibal, M. Dunwell, S. Kattel, E. Stavitski, K. Attenkofer, J. G. Chen, Y. Yan and B. Xu, *J. Am. Chem. Soc.*, 2018, **140**, 13387-13391.
31. H. Jin, L. Li, X. Liu, C. Tang, W. Xu, S. Chen, L. Song, Y. Zheng and S.-Z. Qiao, *Adv. Mater.*, 2019, **31**, 1902709.
32. Y. Luo, G.-F. Chen, L. Ding, X. Chen, L.-X. Ding and H. Wang, *Joule*, 2019, **3**, 279-289.
33. G.-F. Chen, X. Cao, S. Wu, X. Zeng, L.-X. Ding, M. Zhu and H. Wang, *J. Am. Chem. Soc.*, 2017, **139**, 9771-9774.
34. L. Zhang, L.-X. Ding, G.-F. Chen, X. Yang and H. Wang, *Angew. Chem. Int. Ed.*, 2019, **58**, 2612-2616.
35. X. Yu, P. Han, Z. Wei, L. Huang, Z. Gu, S. Peng, J. Ma and G. Zheng, *Joule*, 2018, **2**, 1610-1622.
36. C. Lv, Y. Qian, C. Yan, Y. Ding, Y. Liu, G. Chen and G. Yu, *Angew. Chem. Int. Ed.*, 2018, **57**, 10246-10250.

37. W. Qiu, X.-Y. Xie, J. Qiu, W.-H. Fang, R. Liang, X. Ren, X. Ji, G. Cui, A. M. Asiri, G. Cui, B. Tang and X. Sun, *Nat Commun.*, 2018, **9**, 3485.
38. W.-B. Qiu, Y.-X. Luo, R.-P. Liang, J.-D. Qiu and X.-H. Xia, *Chem. Commun.*, 2019, **55**, 7406-7409.